inorganics

MDPI

Article

Isomeric 4,2′:6′,4′′- and 3,2′:6′,3′′-Terpyridines with Isomeric 4′-Trifluoromethylphenyl Substituents: Effects on the Assembly of Coordination Polymers with [Cu(hfacac)2] (Hhfacac = Hexafluoropentane-2,4-dione)

Giacomo Manfroni, Simona S. Capomolla, Alessandro Prescimone, Edwin C. Constable and Catherine E. Housecroft *

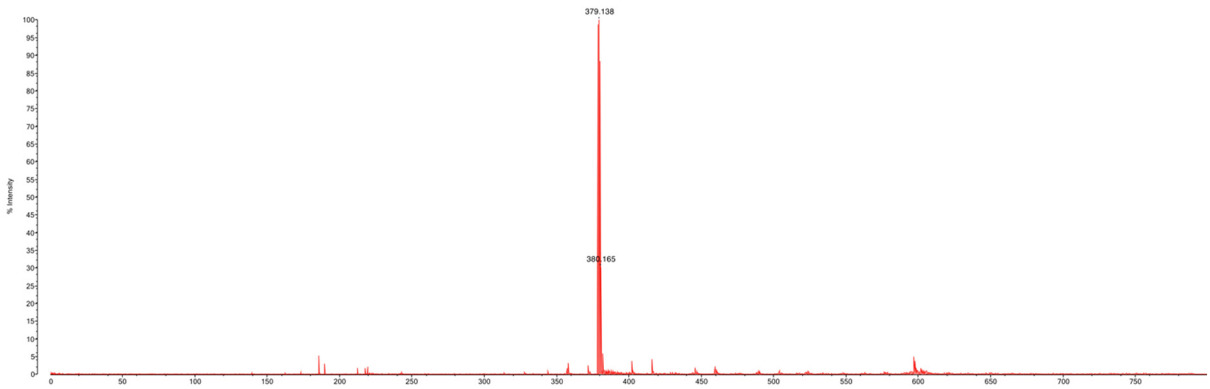

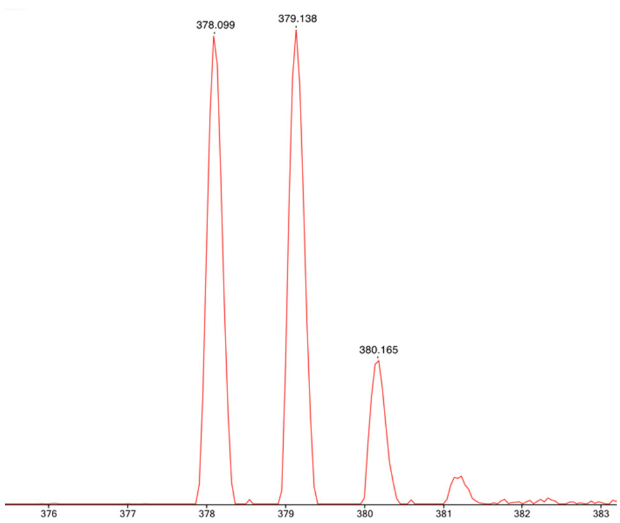

Figure S1. The MALDI-TOF mass spectrum of **1**, and expansion of the base peak.

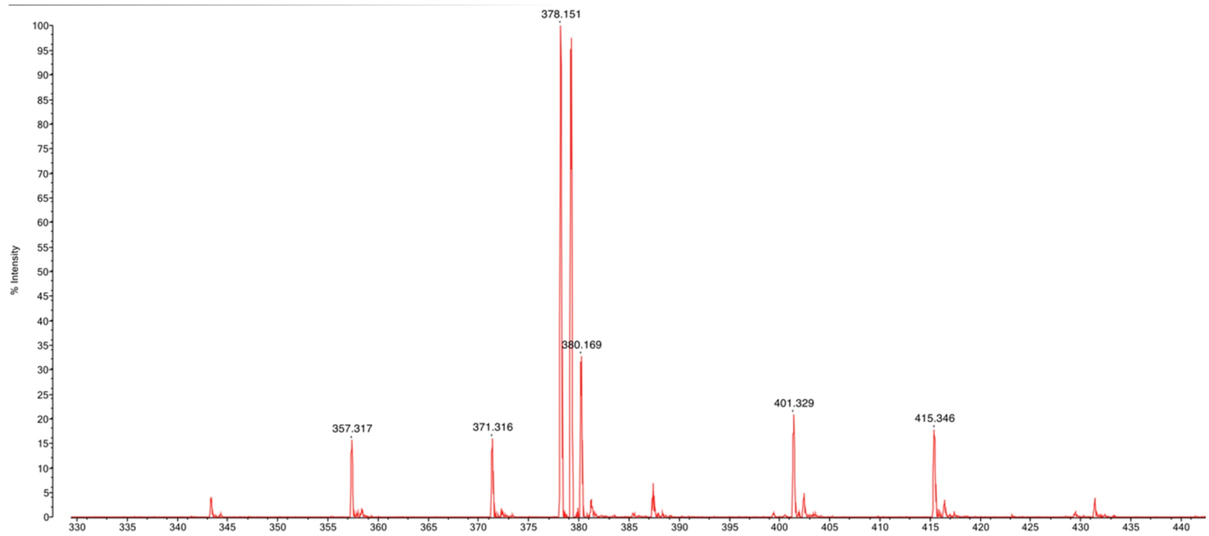

Figure S2. The MALDI-TOF mass spectrum of **2.**

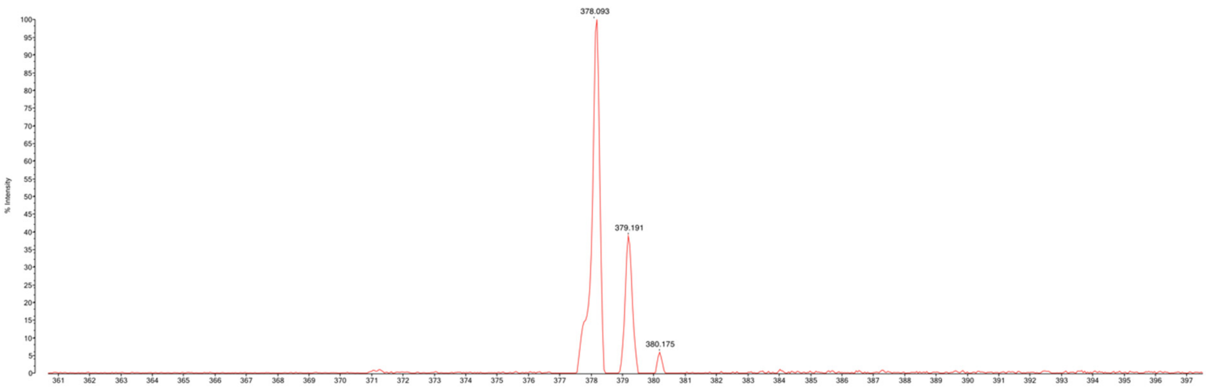

Figure S3. The MALDI-TOF mass spectrum of **3**; expansion of the base peak.

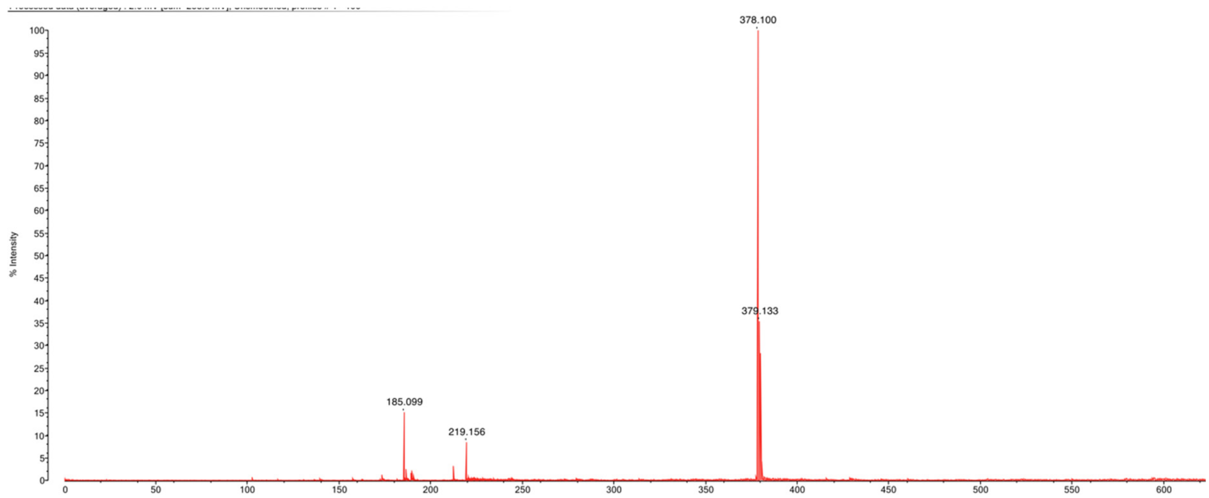

Figure S4. The MALDI-TOF mass spectrum of **4**.

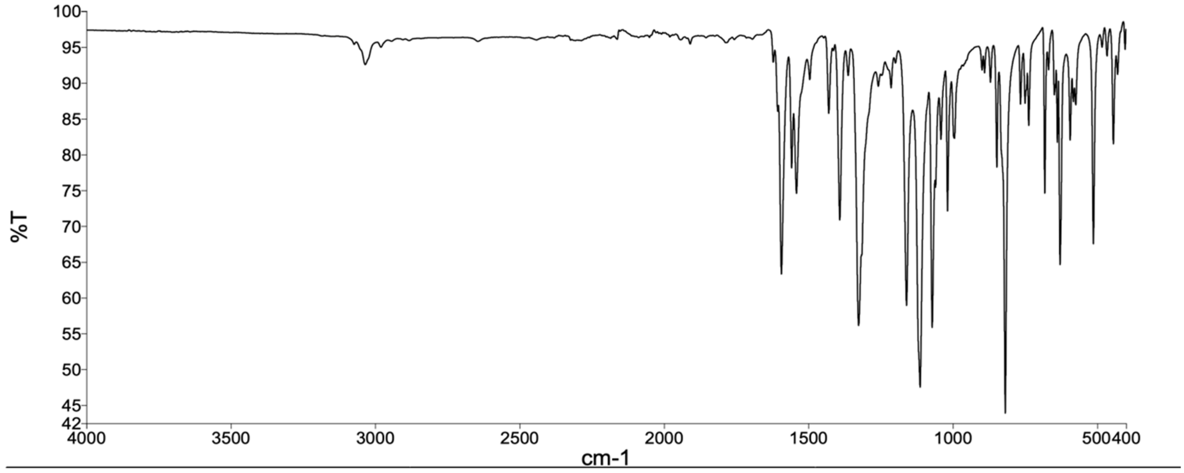

Figure S5. The solid-state FT-IR spectrum of **1**.

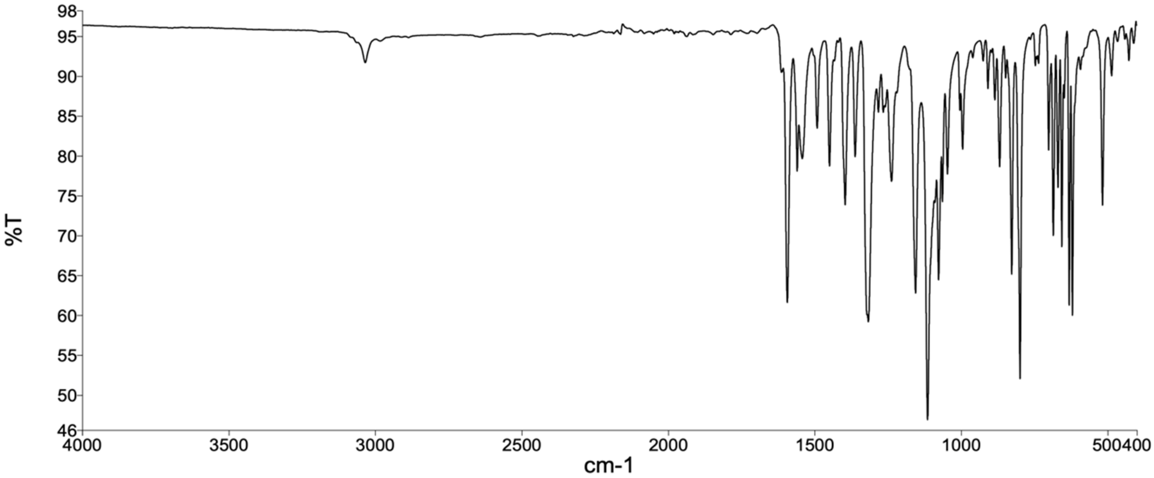

Figure S6. The solid-state FT-IR spectrum of **2.**

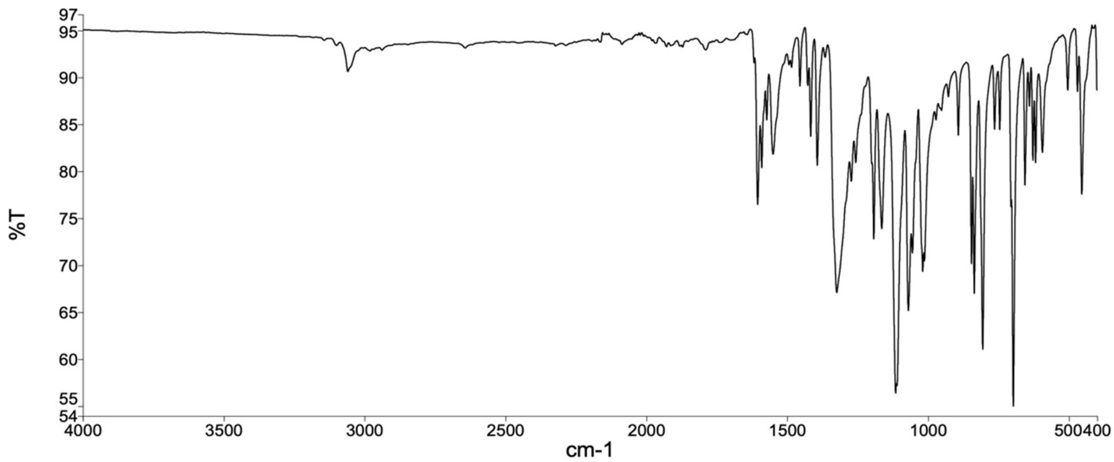

Figure S7. The solid-state FT-IR spectrum of **3**.

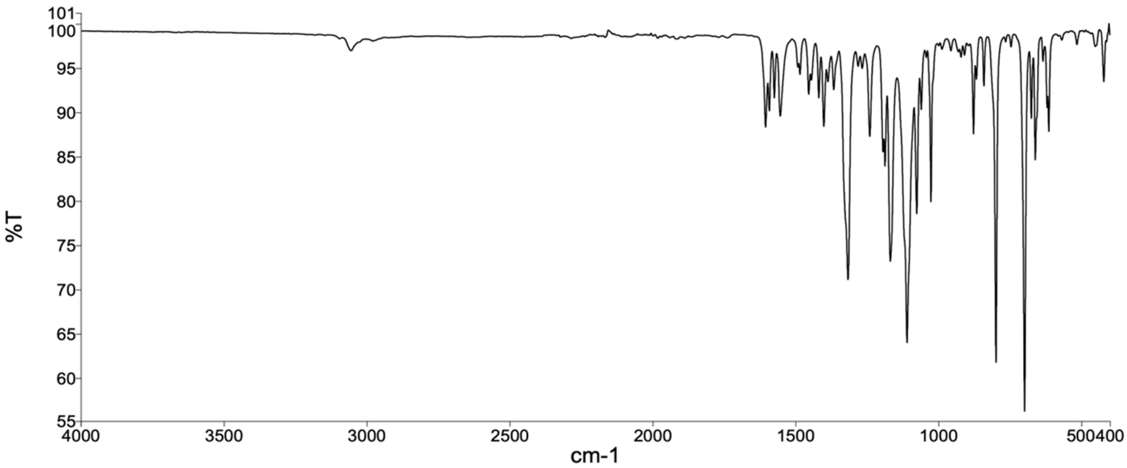

Figure S8. The solid-state FT-IR spectrum of **4**.

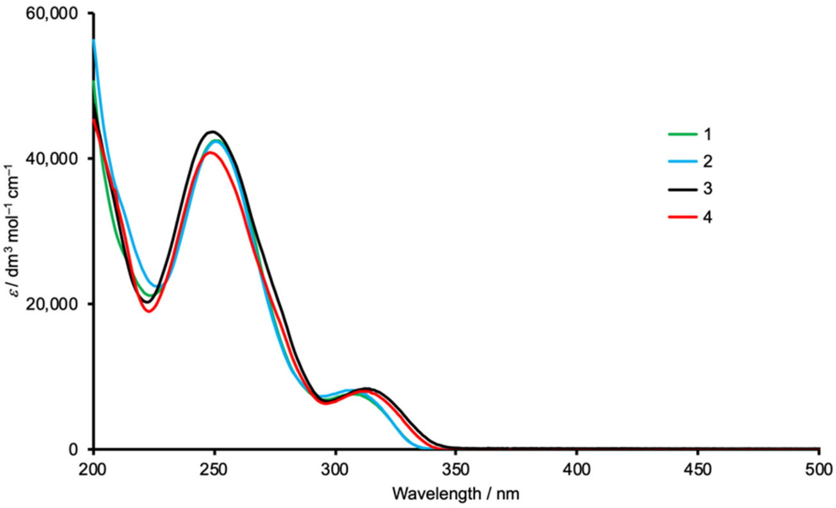

Figure S9. Solution absorption spectra of **1–4** in MeCN (2×10^{-5} mol dm^{-3}).

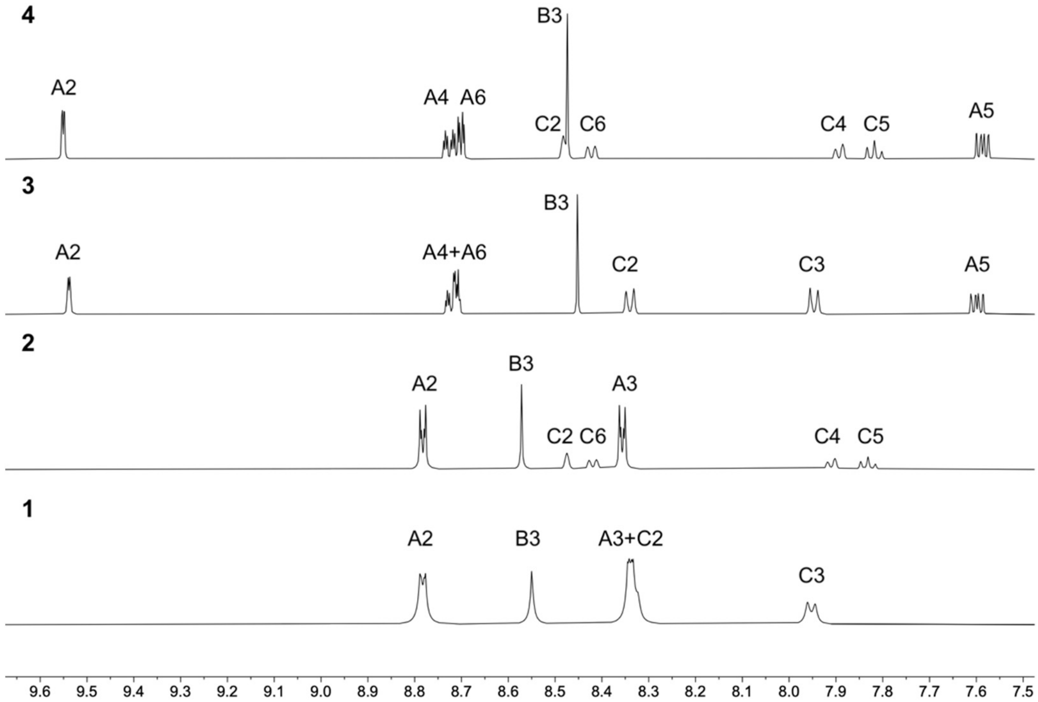

Figure S10. A comparison of the ^{1}H NMR spectra of compounds **1**–**4** (500 MHz, DMSO-d_6, 298 K). See Scheme 3 for atom labels.

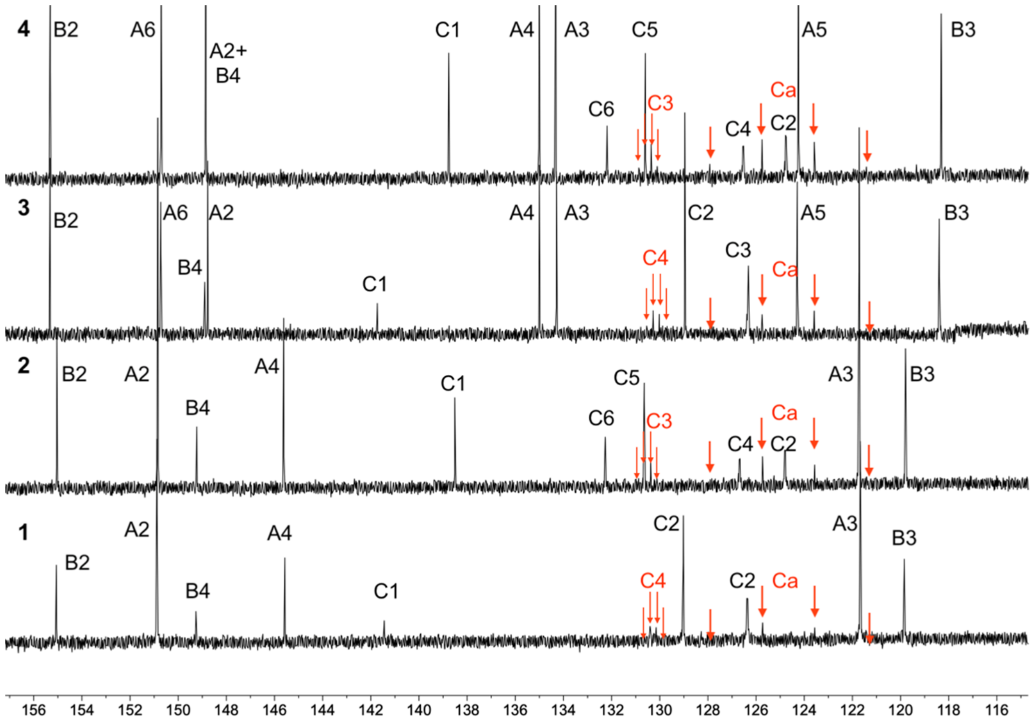

Figure S11. A comparison of the $^{13}C\{^{1}H\}$ NMR spectra of compounds **1**–**4** (126 MHz, DMSO-d_6, 298 K). Quartets (J_{CF}) are emphasized in red. See Scheme 3 for atom labels.

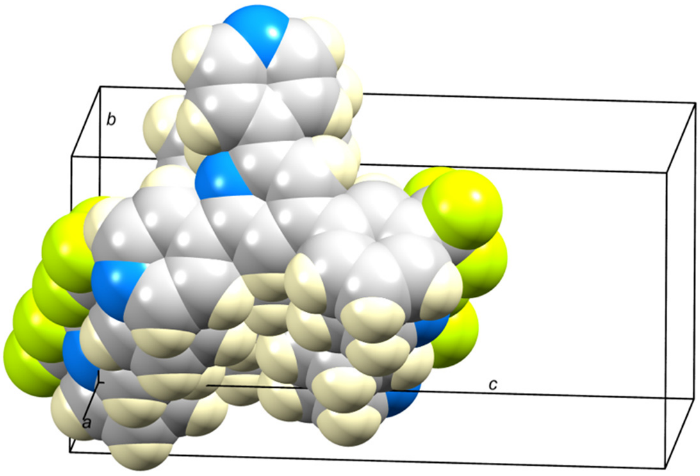

Figure S12. Columnar packing of molecules of **2** with an alternating head-to-tail arrangement.

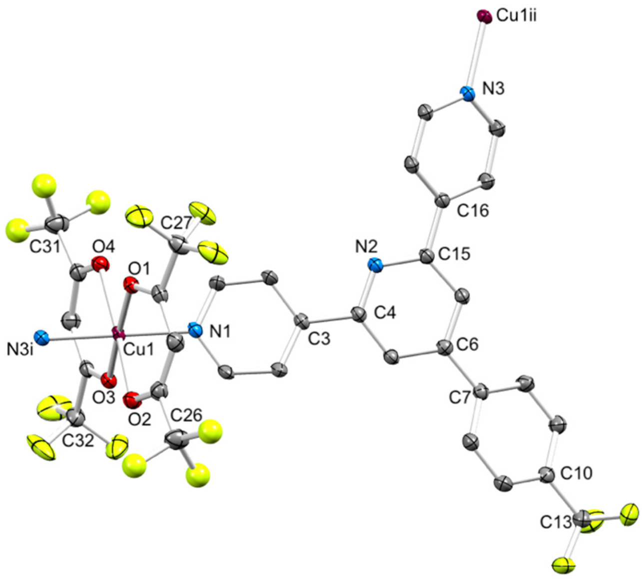

Figure S13. Molecular structure of the asymmetric unit in $[Cu_2(hfacac)_4(\mathbf{1})_2]_n \cdot 2nC_6H_4Cl_2$ with symmetry generated atoms (symmetry codes: i = $^1/_2-x$, $-y$, $-^1/_2+z$; ii = $^1/_2-x$, $-y$, $^1/_2+z$). H atoms and solvent molecules are omitted and ellipsoids are plotted at 40% probability. The CF_3 groups with C26 and C31 were disordered (see Section 3.11) and the F atoms were refined isotropically.

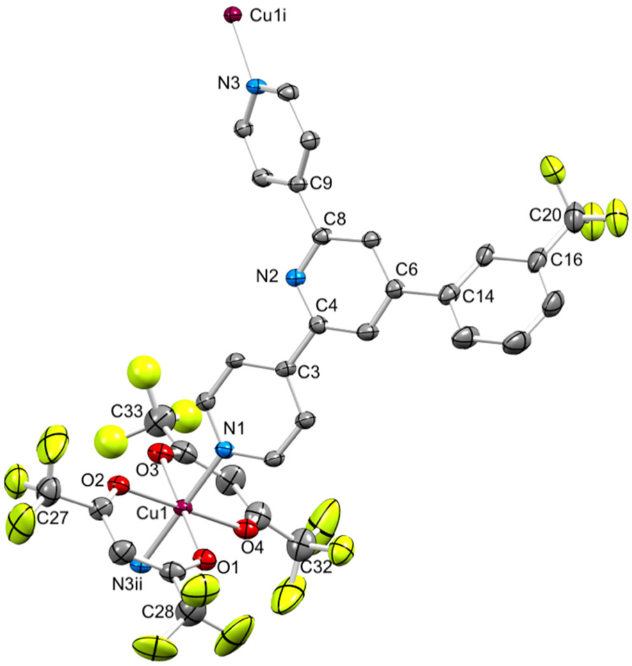

Figure S14. Molecular structure of the asymmetric unit in $[Cu(hfacac)_2(\mathbf{2})]_n \cdot 2nC_6H_5Me$ with symmetry generated atoms (symmetry codes: i = –1+*x*, –1–*y*, –1/2+*z*; ii = 1+*x*, –1–*y*, 1/2+*z*). H atoms and solvent molecules are omitted, and ellipsoids are plotted at 40% probability. The CF_3 group with C33 was disordered (see Section 3.11) and the F atoms were refined isotropically.

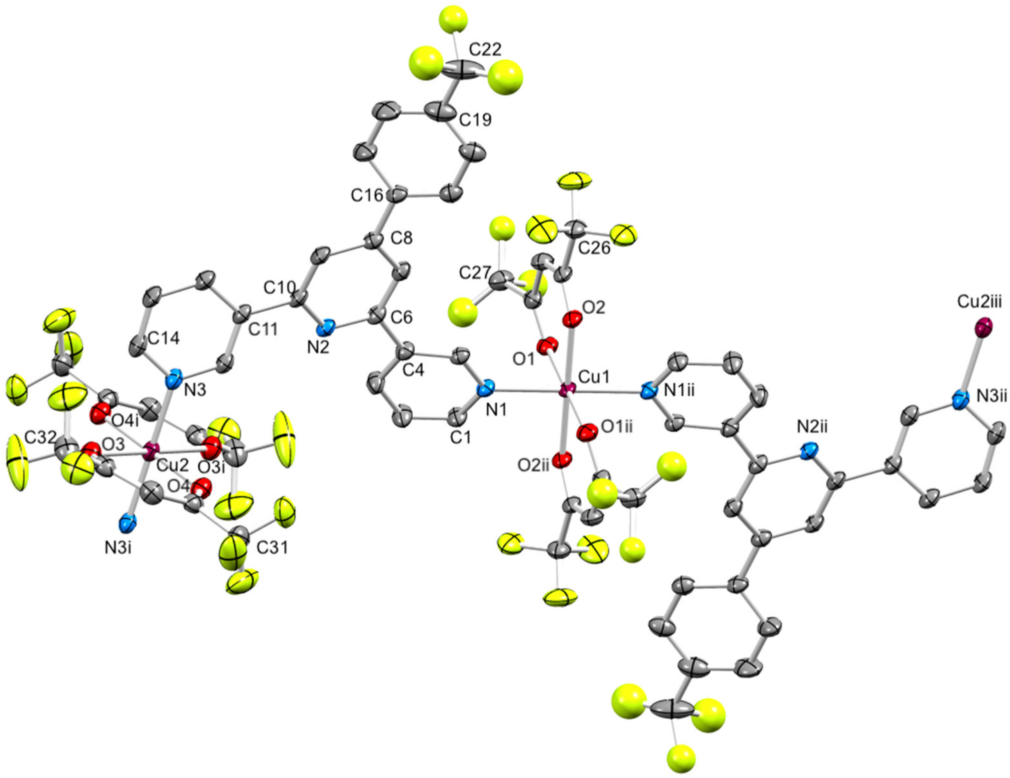

Figure S15. Molecular structure of the asymmetric unit in $[Cu_2(hfacac)_4(\mathbf{3})_2]_n \cdot nC_6H_4Cl_2$ with symmetry generated atoms (symmetry codes: i = 2–*x*, –*y*, –*z*; ii = 1–*x*, 1–*y*, 1–*z*; iii = –1+*x*, 1+*y*, 1+*z*). H atoms and solvent molecules are omitted, and ellipsoids are plotted at 40% probability. The CF_3 groups with C22 and C27 were disordered (see Section 3.11) and the F atoms were refined isotropically.

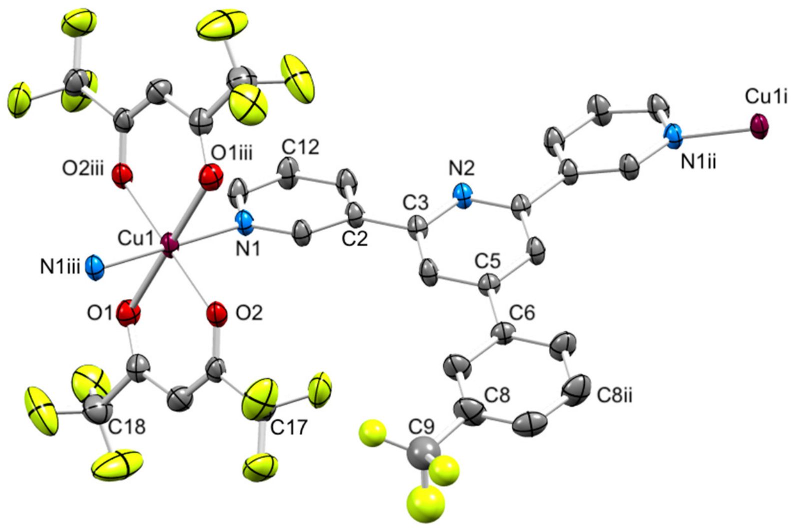

Figure S16. Molecular structure of the asymmetric unit in $[Cu(hfacac)_2(\mathbf{4})]_n{\cdot}nC_6H_5Cl$ with symmetry generated atoms (symmetry codes: i = $1–x$, $^1/_2+y$, $1–z$; ii = x, $^3/_2–y$, z; iii = $1–x$, $1–y$, $1–z$). H atoms are omitted, and ellipsoids are plotted at 40% probability. The CF_3 group with C9 is disordered over two sites related by a mirror (see Section 3.11) and was refined isotropically; only one position is shown.

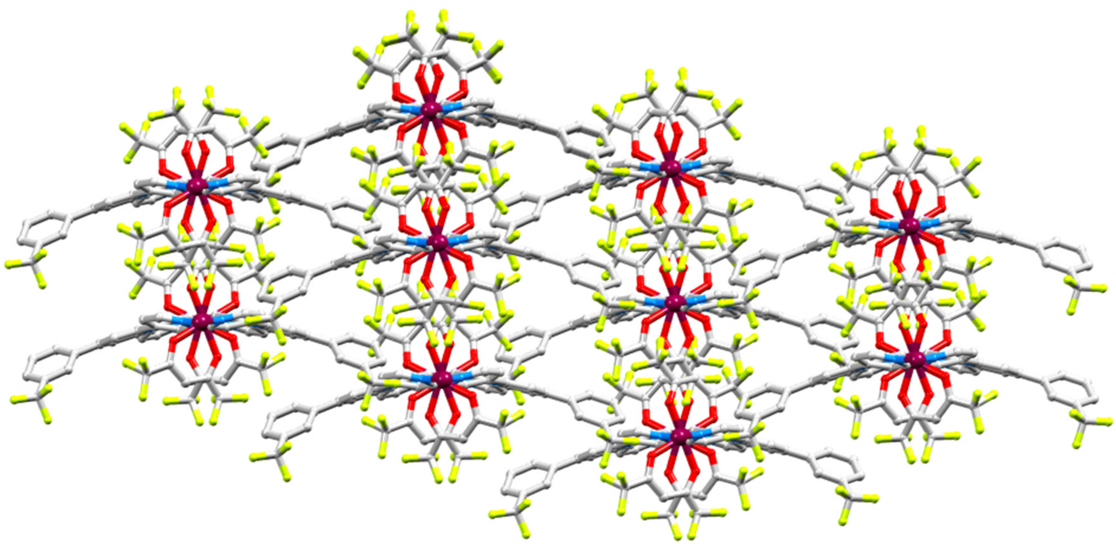

Figure S17. Looking along the polymer chains in $[Cu(hfacac)_2(\mathbf{2})]_n{\cdot}2nC_6H_5Me$ to illustrate that the 1D-polymers are arranged parallel to one another.

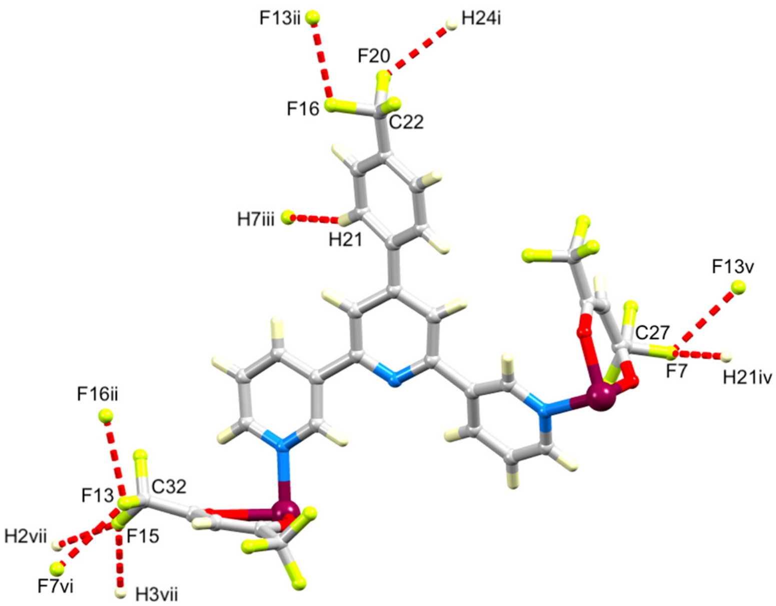

Figure S18. Extensive C–F...F–C and C–F...H–C contacts are present in $[Cu_2(hfacac)_4(\mathbf{3})_2]_n \cdot nC_6H_4Cl_2$. Symmetry codes: i = 2–*x*, 1–*y*, 2–*z*; ii = 3–*x*, 1–*y*, 1–*z*; iii = 1+*x*, *y*, *z*; iv = –1+*x*, *y*, *z*; v = –1+*x*, *y*, 1+*z*; vi = 1+*x*, *y*, –1+*z*; vii = 2–*x*, –*y*, –*z*. Contact distances: F...F = 2.85 and 2.87 Å; H...F in the range 2.50–2.65 Å. Longer contacts have been ignored.

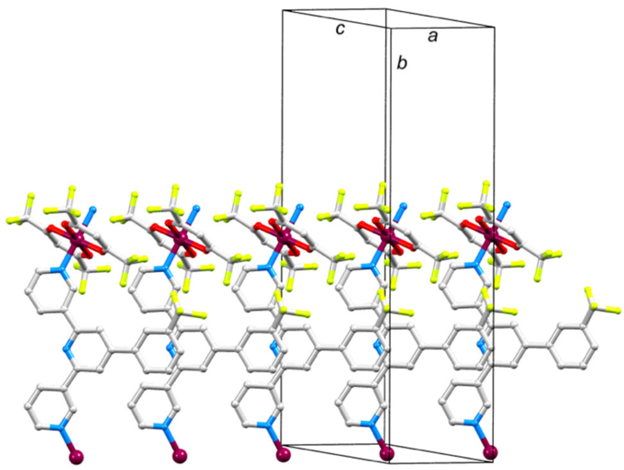

Figure S19. Infinite stacks of 3,2':6',3''-tpy domains interconnect 1D-polymer chains in $[Cu(hfacac)_2(\mathbf{4})]_n \cdot nC_6H_5Cl$. See also Figure 8c.

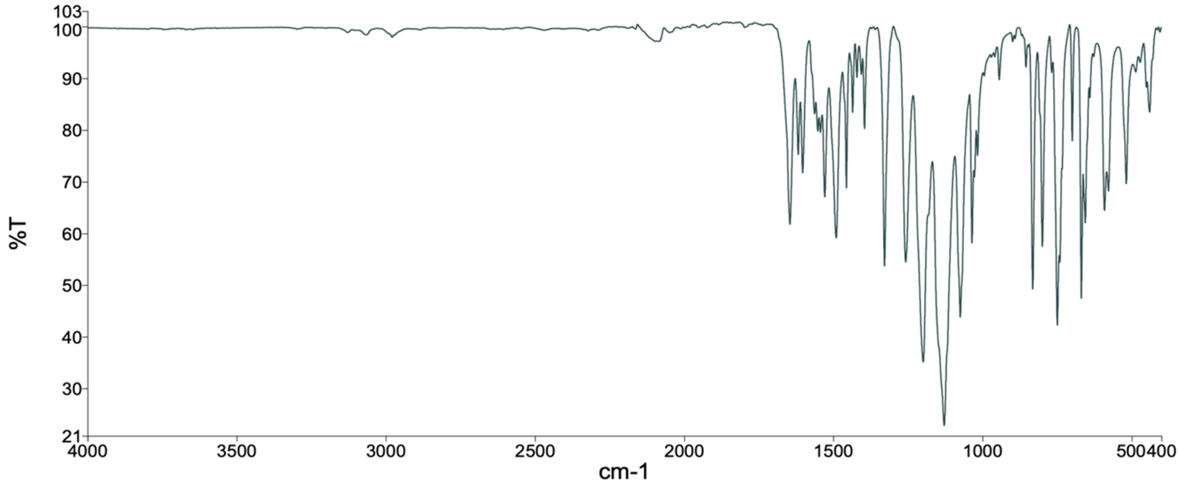

Figure S20. The solid-state IR spectrum of $[Cu_2(hfacac)_4(\mathbf{1})_2]_n \cdot 2nC_6H_4Cl_2$.

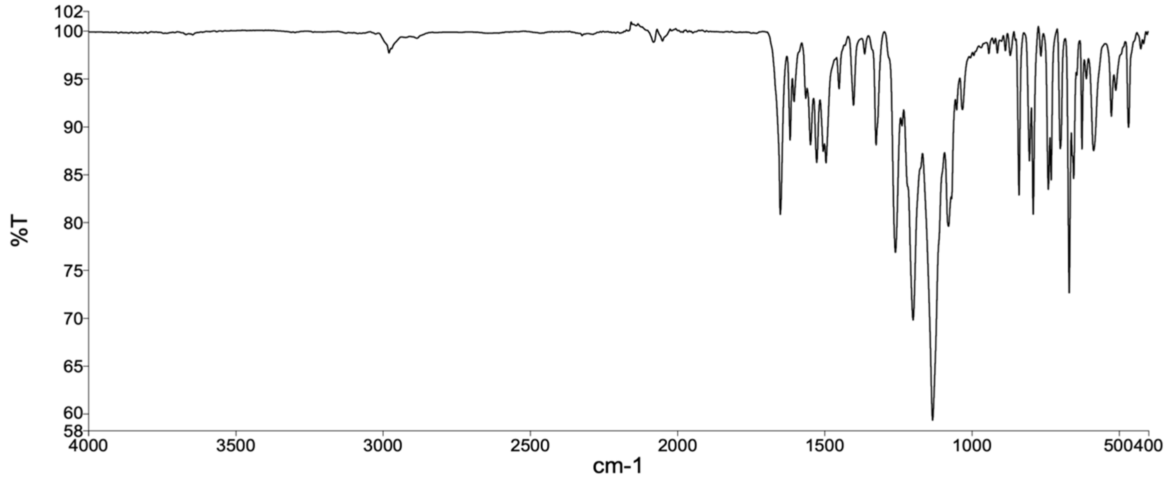

Figure S21. The solid-state IR spectrum of $[Cu(hfacac)_2(\mathbf{2})]_n \cdot 2nC_6H_5Me$.

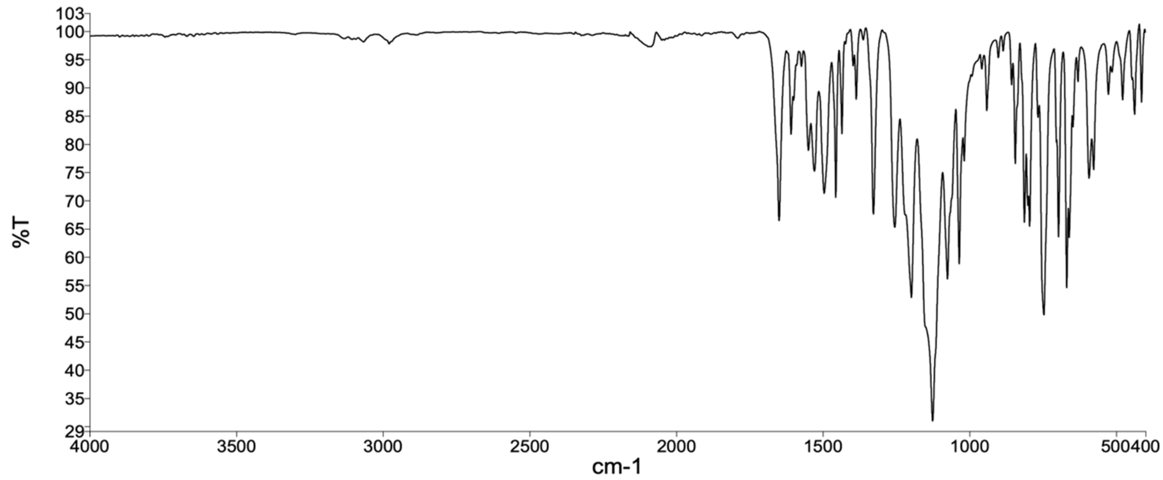

Figure S22. The solid-state IR spectrum of $[Cu_2(hfacac)_4(\mathbf{3})_2]_n \cdot nC_6H_4Cl_2$.

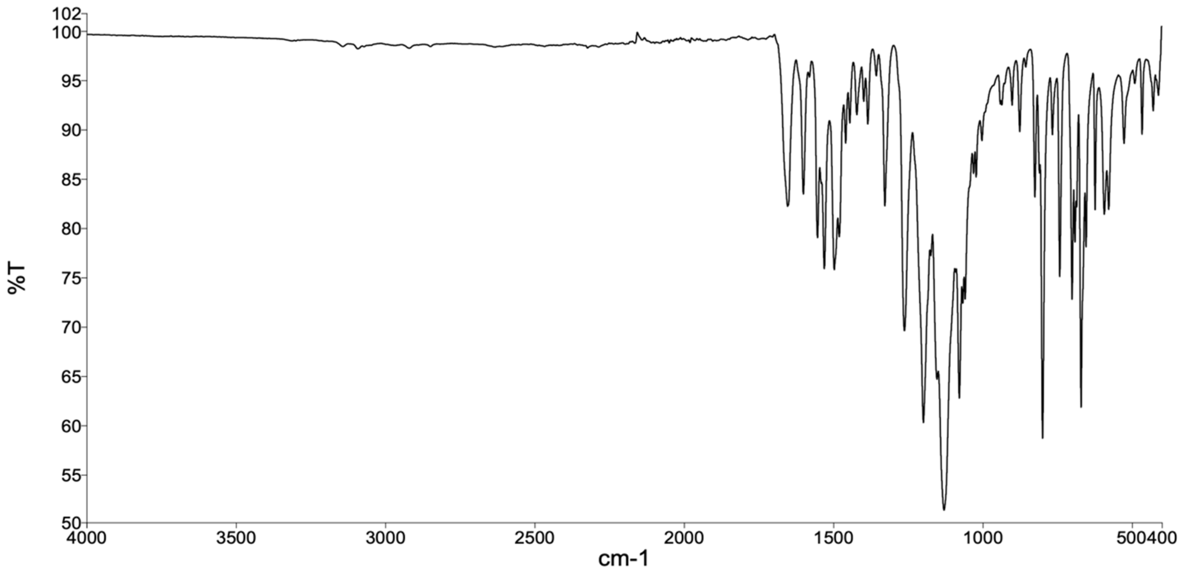

Figure S23. The solid-state IR spectrum of $[Cu(hfacac)_2(\mathbf{4})]_n{\cdot}nC_6H_5Cl$.

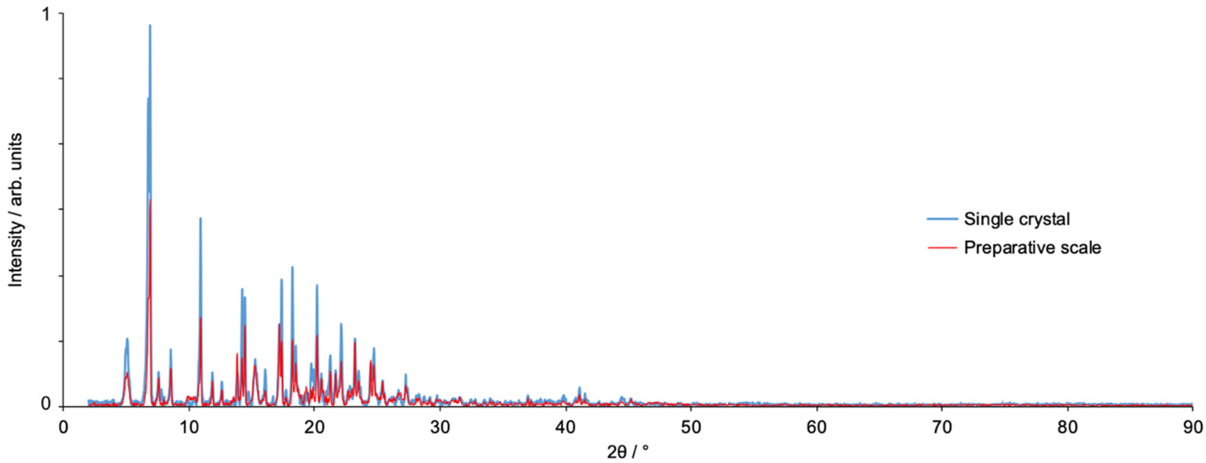

Figure S24. A comparison of the PXRD pattern of $[Cu_2(hfacac)_4(\mathbf{2})_2]_n$ prepared on a preparative scale, and the pattern from the bulk single crystals of $[Cu(hfacac)_2(\mathbf{2})]_n{\cdot}2nC_6H_5Me$. The difference in solvent arises from drying the synthesized sample. The single crystals were not dried and were ground before PXRD.

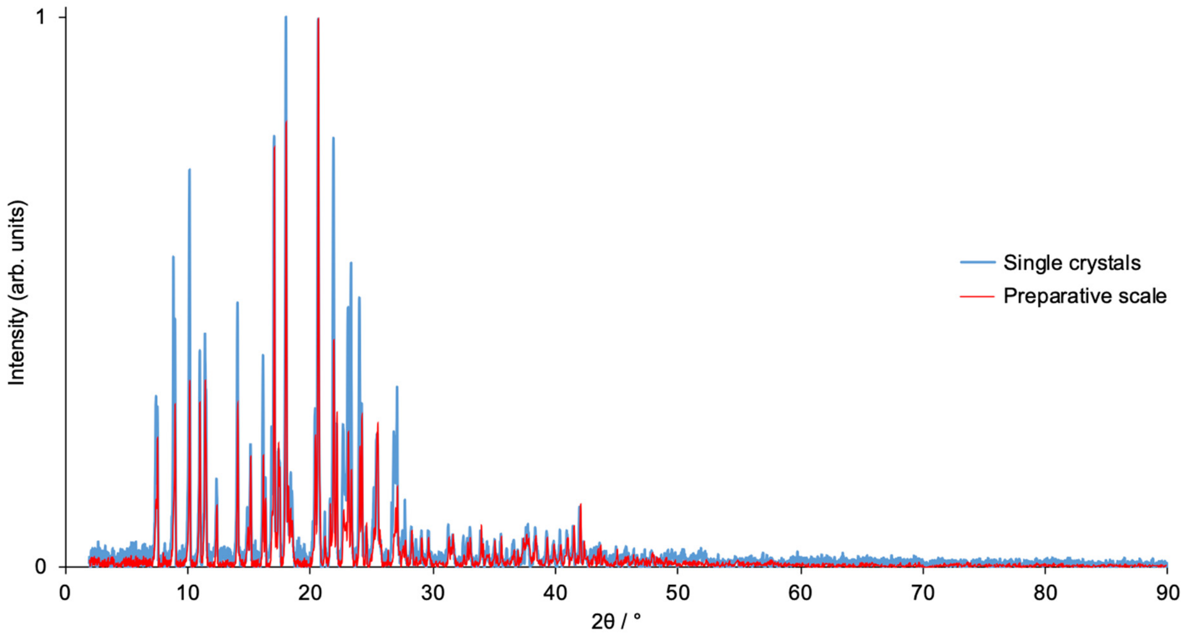

Figure S25. A comparison of the PXRD pattern of $[Cu_2(hfacac)_4(\mathbf{3})_2]_n$ prepared on a preparative scale, and the pattern from the bulk single crystals of $[Cu_2(hfacac)_4(\mathbf{3})_2]_n{\cdot}nC_6H_4Cl_2$. The difference in solvent arises from drying the synthesized sample.

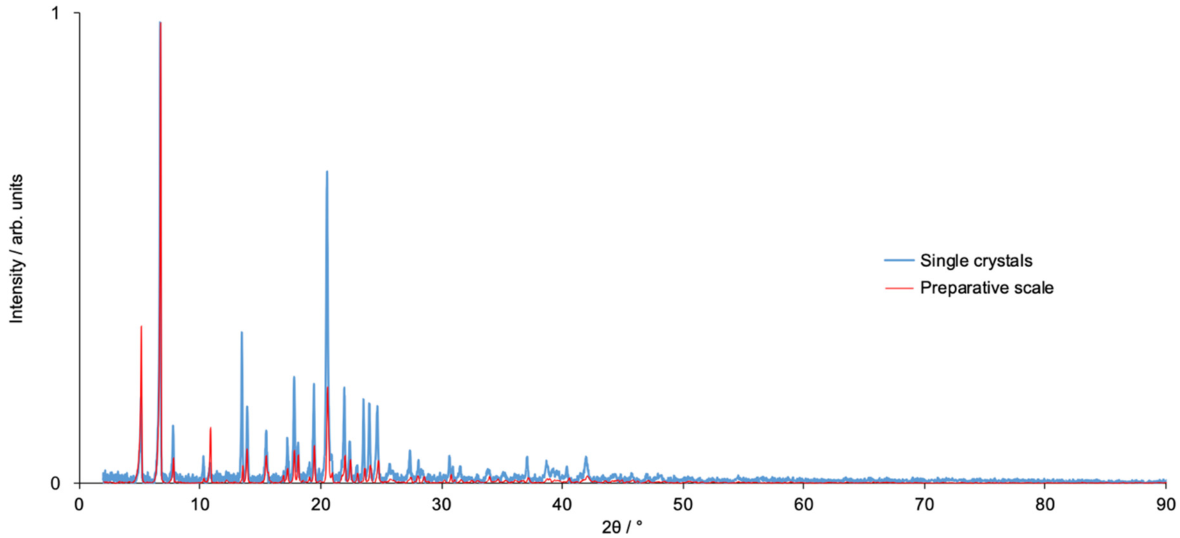

Figure S26. A comparison of the PXRD pattern of $[Cu_2(hfacac)_4(\mathbf{4})_2]_n$ prepared on a preparative scale, and that from the bulk single crystals of $[Cu_2(hfacac)_4(\mathbf{4})_2]_n{\cdot}nC_6H_5Cl$. The difference in solvent arises from drying the synthesized sample.